Paper Number 01ICES-2363

Shuttle Spacesuit (Radiation) Model Development

Brooke M. Anderson
George Washington University, Hampton, VA

J. E. Nealy
Old Dominion University, Norfolk, VA

G.D.Qualls, P.J. Staritz, J.W.Wilson
NASA Langley Research Center, Hampton, VA

M.-H. Y. Kim
College of William and Mary, Williamsburg, VA

F. A. Cucinotta
NASA Johnson Space Center, Houston, TX

W. Atwell
The Boeing Co. Houston, TX

G. De Angelis
NASA Langley Research Center, Hampton, VA
& Istituto Superiore di Sanita', Rome, Italy

J. Ware, A. E. Persans
ILC Dover, Frederica, DE

ABSTRACT

A detailed spacesuit computational model is being developed at the Langley Research Center for exposure evaluation studies. The details of the construction of the spacesuit are critical to an estimate of exposures and for assessing the health risk to the astronaut during extra-vehicular activity (EVA). Fine detail of the basic fabric structure, helmet, and backpack is required to assure a valid evaluation. The exposure fields within the Computerized Anatomical Male (CAM) and Female (CAF) are evaluated at 148 and 156 points, respectively, to determine the dose fluctuations within critical organs. Exposure evaluations for ambient environments will be given and potential implications for geomagnetic storm conditions discussed.

INTRODUCTION

The International Space Station will require 1500 hours of Extra-Vehicular Activity (EVA) during its construction and 400 hours of EVA per year in operations and maintenance. The 51.6º inclination of the ISS orbit provides a highly variable radiation environment driven by solar activity. Solar particle events will adversely impact the radiation environment in this region, especially in the case of an associated geomagnetic storm during which the region of polar cap is expanded during the storm main phase [1]. The geomagnetic storm conditions also increase the strength of the trapped electron environment by up to four orders of magnitude; this electron enhancement can persist for several days. Even under quiet field conditions, the distribution of dose within the body during EVA is vastly different than that experienced within the ISS and dose gradients near the body surface are important to the evaluation of effective dose as related to cancer risks. This gradient is related to the material make-up of the spacesuit about critical body organs and enhancements of the electron environment during times of geomagnetic activity.

There are two spacesuits in current usage within the space program: Shuttle Spacesuit [2] and Orlan-M Spacesuit [3,4]. The shuttle spacesuit components are discussed elsewhere [2,5,6] and serve as a guide to development of the current model. The present model is somewhat simplified in details which are considered to be of second order in their effects on exposures. A more

systematic approach is ongoing on a part-by-part basis with the most important ones, in terms of exposure contributions, being addressed first with detailed studies of the relatively thin spacesuit fabric as the first example [7]. Additional studies to validate the model of the head coverings (bubble, helmet, visors,…) will be undertaken in the near future. The purpose of this paper is to present the details of the model as it is now and to examine its impact on estimates of astronaut health risks. In this respect, the nonuniform distribution of mass of the spacesuit provides increased shielding in some directions and some organs. These effects can be most important in terms of health risks [8] and especially critical to evaluation of potential early radiation effects [9] under extreme but unusual event exposures.

SPACESUIT DESCRIPTION

The basic spacesuit assembly is shown in figure 1. The Liquid Cooling and Ventilation Garment (LCVG) fits close to the body and is constructed of Spandex, Nylon net, and ethylvinylacetate tubing filled with circulating water. The areal density of the Spandex/Nylon net is 0.034 g/cm^2 and the 4mm o.d. tube is 0.078 g/cm (including water) and they are inserted in the Spandex at the rate of 1+ tubes per centimeter (figure 2). The usual approximation of the LCVG material is then 0.154 g/cm^2 as used by Kosmo et al. [5]. The inadequacy of this approximation is thoroughly discussed in [7]. The Communications Carrier Assembly (CAA) is currently not represented in the model. The helmet with its internal vent deflector is constructed of polycarbonate as is the protective visor of the Extra-Vehicular Visor Assembly (EVVA). The remaining visors are constructed of polysulfone. The assembly has an inner teflon liner and is covered by an Orthofabric for mechanical protection, aluminized Mylar for thermal insulation, and Dacron. The material list is given in table 1.

Table 1. Material lay-up of helmet and EVVA.

Layer	**Material**	**Areal density, g/cm^2**
Outer layer	Orthofabric-Teflon/Nomex/Kevlar	0.049
Insulation	Aluminized Mylar- 5 plys	0.014
Spacer	Dacron fiber- 5 plys	0.011
Inner liner	Teflon	0.028
EVVA shell	Polycarbonate	0.381
Sun visor	Polysulfone	0.190
Eye shade	Polysulfone	0.190
Protective visor	Polycarbonate	0.182
Helmet	Polycarbonate	0.182

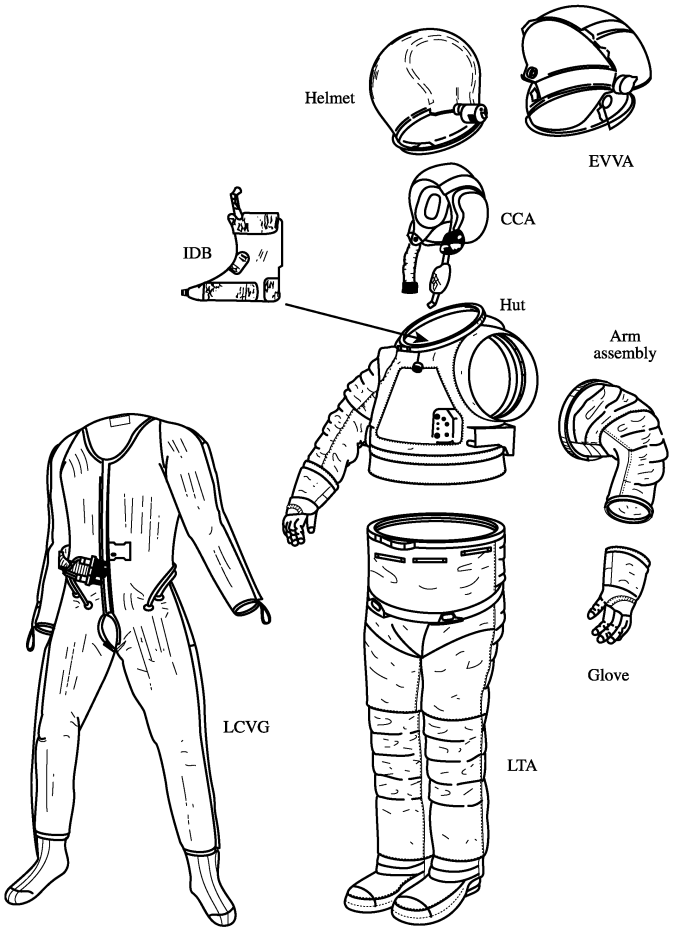

Fig. 1. Basic components of the Shuttle spacesuit.

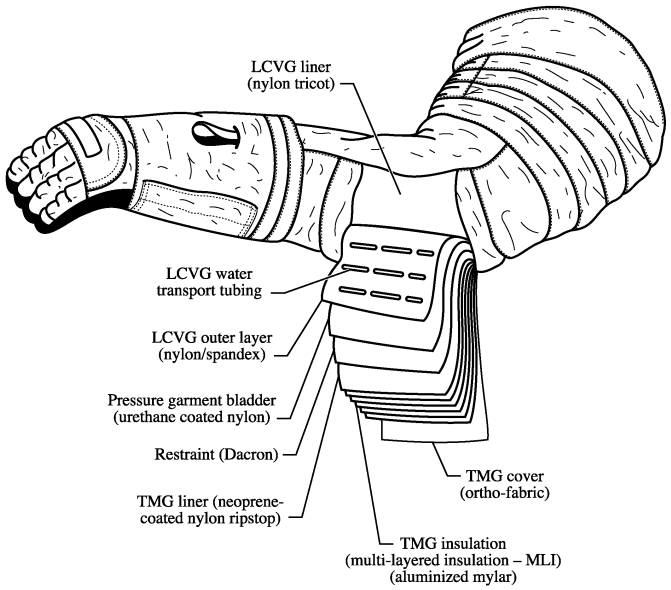

Fig. 2. Cross section of material lay-up.

The remainder of the suit consists of the Hard Upper Torso (HUT), the arm assembly including glove, and the Lower Torso Assembly (LTA). The HUT main body is constructed with Fiberglas and covered outside with Orthofabric, aluminized Mylar, and Neoprene coated Nylon ripstop. Under the HUT is the LCVG next to the astronaut body. The material lay-up in the HUT region of the suit is given in table 2. The arm assembly and LTA

are made of fabric and water filled cooling tubes. The fabric lay-up is shown in figure 2 and given in table 3 and discussed in [6]. The fabrics of the arm assembly and LTA, gloves, and boots are given a simplified representation in the present model. For example, there is additional fabric in locations where bending occurs to allow flexibility. These will be modeled later in the next level of detail.

An important component of the spacesuit shield model is the Portable Life Support System (PLSS) shown in figure 3. Not shown in the figure are the secondary oxygen tanks which attach to the lower section of the PLSS. Approximate estimates of material mass of various subsystems and overall dimensions are given in table 4. As seen in the table, a major fraction of the mass of the Extravehicular Maneuvering Unit (EMU) is associated with the backpack and is expected to be important in providing protection to internal organs.

Table 2. Material lay-up of the Hard Upper Torso (HUT).

Layer	**Material**	**Areal density, g/cm^2**
Outer layer	Orthofabric-Teflon/Nomex/Kevlar	0.049
Insulation	Aluminized Mylar- 5 plys	0.014
Inner liner	Neoprene coated Nylon ripstop	0.028
Hard shell	Fiberglas	0.354
LCVG	Spandex/water/ ethylvinylacetate	0.154

Table 3. Material lay-up of the spacesuit fabric and water filled tube [2,7].

Material	**Areal density, g/cm^2**
Orthofabric-Teflon/Nomex/Kevlar	0.049
Reinforced aluminized Mylar	0.014
Neoprene coated ripstop	0.028
Dacron® Polyester	0.021
Urethane Coated Nylon	0.014
Nylon/Spandex/water/ethylvinylacetate	0.154

The geometric arrangement of materials in tables 1-4 will then provide a preliminary model of the spacesuit. Although the description is somewhat simplified, this is the most complete shielding model to date. This is an important step in understanding the expected exposures in ISS operations and will be useful in mission planning.

SPACESUIT MODEL

The preliminary spacesuit model is implemented using the CAD geometry package of IDEAS[2] software. The geometry is simplified but represents the location of major massive components and the distribution of fabric and other components about the astronaut position within the suit cavity. The CAD derived model is shown in figure 4.

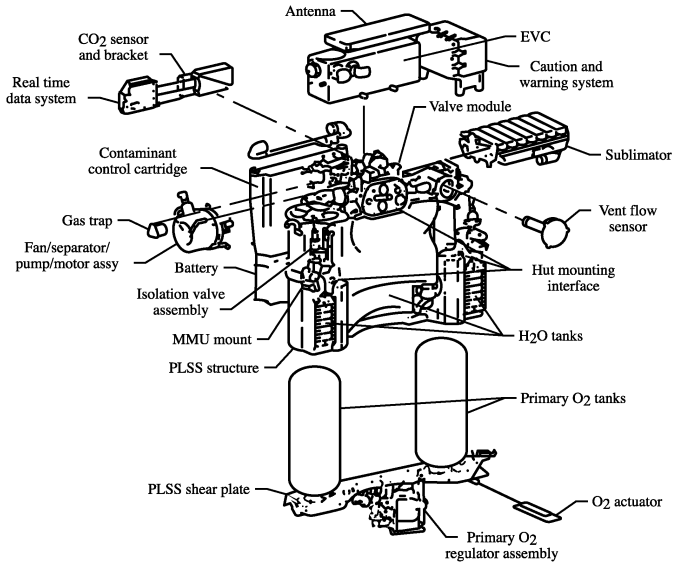

Fig. 3. EMU Portable Life Support System (PLSS).

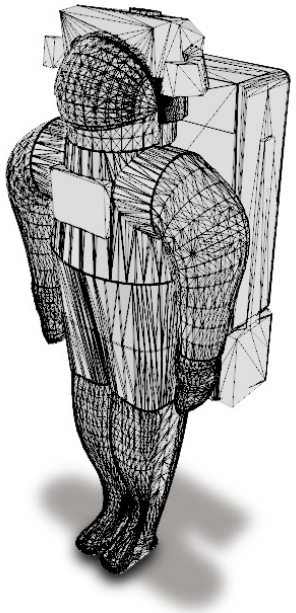

Fig. 4. CAD model in faceted representation.

Table 4. Approximate material and dimensions of PLSS.

Subsystem	Materials	Mass, kg	Dimensions, inch (h,w,d)
O_2 Ventilating Circuit:			
Regulators, vessels, fans…	Fe. Cr. Ni, Cu,…	14.4	
LiOH assembly	LiOH, Fe	6.4	
H_2O transport:			
Pump, valves, sensors	Fe, Cu	6.5	
liquid	H_2O	4.5	
Electrical sys.			
Electronics	Si, O, Cu…	15.1	
battery	ZnAgO	4.5	
O_2 purge sys.			
Bottles	Fe, O	8.6	
regulator	Fe	4.2	
Total		65.2	25 x 23 x 7

In the model, it is assumed that the Spandex/Nylon net of the LCVG is part of the remaining suit fabric and that the ethylvinylacetate tubes filled with water are lying on the skin surface except for the head, hands, and feet. In testing it is found that the fabric of table 3 (less the water filled tube) presents a distribution [7] of material along a given path which is random according to

$$p(t) = exp[-(t-t_o)^2/(2\sigma^2)]/(2\pi\sigma^2)^{1/2} \quad (1)$$

where the mean thickness t_o is 0.161 g/cm^2 and σ is 0.03 g/cm^2. It is assumed that each ray through the fabric is scaled according to the distribution (1). In the CAD model the fabric is of fixed thickness t_{min} but rays passing through the surface in direction $\boldsymbol{\Omega}$ see thickness along the slant height $t_m(\boldsymbol{\Omega})$ and needs relation to the fabric distribution (1). The ray thickness is then taken as a random variable in which

$$t_{ray}(\boldsymbol{\Omega}) = t(\kappa) t_m(\boldsymbol{\Omega}) / t_{min} \quad (2)$$

where κ is a uniform random number on the interval {0,1} and

$$t(\kappa) = t_o + 2^{1/2}\ \sigma\, erf^{-1}(2\kappa - 1) \quad (3)$$

where erf^{-1} is the inverse error function and a different random number κ is taken for each ray direction. The scaling in equation (2) represents the nonuniformity in the fabric observed in transmission testing [7].

The water-filled tubes are likewise complicated in their representation within the CAD model. The tubes are located in parallel arrays separated by 1-centimeter [7]. Since the tubes are held on the skin of the astronaut (represented by the CAM or CAF models) and an arbitrary point in the astronaut's body at which the exposure is to be evaluated can be considered randomly, then the problem is to find the probability that the rays passing through the dose point in fact passed through a section of a water-filled tube. The tubes are mainly important to the skin points located near a tube. Points remote from any tube (e.g., deep in the body) are little affected. Since the tubes are parallel and 1 centimeter apart, then each point will only consider the two nearest tube pairs. This is accomplished as follows.

The nearest tube to the dose point will lie near the ray of minimum distance to the surface of the skin. This ray direction $\boldsymbol{\Omega}_{min}$ is found by searching over the body thickness function $t_b(\boldsymbol{\Omega})$ for the smallest value. At that point on the surface with minimum thickness to the dose point we place two tubes on opposite sides one located at a distance $x(\kappa)$ given as

$$x(\kappa) = 0.5\ \kappa\ (cm) \quad (4)$$

where the second tube is at a distance $1 - x(\kappa)$ and κ is a uniformly distributed random number on the interval {0,1} as before. However, whereas each direction $\boldsymbol{\Omega}$ has a separate κ in equation (2), there is only one κ for each dose point in equation (4). For a given $x(\kappa)$ and direction $\boldsymbol{\Omega}$ we require the chord through either of the two tubes. To calculate this chord, we require solving the appropriate geometry. The first is to define a coordinate system. Since $\boldsymbol{\Omega}_{min}$ is assumed normal to the local surface then any unit vector $\boldsymbol{\beta}$ such that $\boldsymbol{\beta}\cdot\boldsymbol{\Omega}_{min} = 0$ is tangent to the local surface. We will use an arbitrary tangent vector to define the direction to the tube and a unit vector $\boldsymbol{\gamma}$ parallel to the tube axis for the calculations. We take

$$\boldsymbol{\beta}\cdot\boldsymbol{\Omega}_{min} = \beta_1\alpha_1 + \beta_2\alpha_2 + \beta_3\alpha_3 = 0 \quad (5)$$

which we solve by finding $\alpha_{lm} = min\{\alpha_l\}$ and set $\beta_{lm} = 0$. The remaining β_l can be solved with the requirement of normalization to unity. The vector parallel to the tube is given as

$$\boldsymbol{\gamma} = \boldsymbol{\beta} \times \boldsymbol{\Omega}_{min} \quad (6)$$

The point on the tube axis located at $x(\kappa)$ along the surface nearest the dose point as defined above is

$$\boldsymbol{x}_{tube} = t(\boldsymbol{\Omega}_{min})\ \boldsymbol{\Omega}_{min} + x(\kappa)\boldsymbol{\beta} \quad (7)$$

An arbitrary point on the tube axis is given as

$$\boldsymbol{x}(s) = \boldsymbol{x}_{tube} + s\ \boldsymbol{\gamma} \quad (8)$$

where s is the distance along the tube measured from the point on the tube nearest the dose point. We need the nearest point to the tube axis along an arbitrary direction $\boldsymbol{\Omega}$ to evaluate the chord for that ray. This is accomplished by finding the minimum of the distance D as

$$D^2 = Min_{s,v}\ \{ [\boldsymbol{x}(s) - v\ \boldsymbol{\Omega}]^2 \} \quad (9)$$

The solution can be written as

$$D^2 = [t(\boldsymbol{\Omega}_{min}) - v\ \omega_1]^2 + [x(\kappa) - v\ \omega_2]^2 \quad (10)$$

where

$$v = [t(\boldsymbol{\Omega}_{min})\ \omega_1 + x(\kappa)\ \omega_2]/[\ \omega_1^2 + \ \omega_2^2] \quad (11)$$

The chord is, for D less than the tube radius r_0, given as

$$C = 2\ [r_o^2 - D^2]^{1/2} \quad (12)$$

and has value zero for values of D greater than r_o. The material the ray must penetrate to reach the astronaut within the suit is the chord so that the total shielding is

$$t_{ray}(\boldsymbol{\Omega}) = t(\kappa)t_m(\boldsymbol{\Omega})\ /t_{min} + C \quad (13)$$

Note, even if an intersection of the tube at $x(\kappa)$ is not found the calculation is to be repeated by replacing $x(\kappa)$ with $x(\kappa)$ - *1* for the second tube of the nearest pair. The chord of the next nearest pair is evaluated by replacing the $x(\kappa)$ by $x(\kappa)$ + 1 and then by $x(\kappa)$ -2. The appropriate value(s) of C is (are) used (summed) in equation (13).

The CAD model of the spacesuit is used to generate shielding distributions about the dose points chosen in the CAM and CAF models and will be modified according to the above analysis to represent the materials about the dose points.

HUMAN GEOMETRY MODEL

The Computerized Anatomical Male (CAM) model was first developed by Kase [10] in 1970. Numerous errors were discovered in the combinatorial geometry, and Billings and Yucker [11] corrected the geometrical representation in 1973 using a QUAD geometry modeling technique [12] where geometrical regions and surfaces are used to represent the 50th percentile US Air Force male. The model is very detailed comprising some 1100 unique geometric surfaces and approximately 2400 solid regions. The internal body geometry such as critical body organs, voids, bone, and bone marrow are explicitly modeled with the proper chemical composition and density. A supporting computer program called CAMERA was developed to perform analyses on the model, which include ray tracing to generate shielding distributions for any point in and on the CAM model. CAMERA also has the capability to generate cross-sectional views of the coordinate (dose) point of interest.

With the increase of females being assigned to fly on Shuttle missions, Yucker and Huston [13] developed the Computerized Anatomical Female (CAF) model. Using the existing CAM model, they "removed" the male organs and "replaced" them with the appropriate female organs (breast, uterus, and ovaries). Since the average female is approximately 92% the size of the average male, the CAF was scaled accordingly.

Since astronauts come in all sizes, Yucker [14] developed a 3-D scaling capability, and Atwell [15,16] later refined and made several corrections to the CAF model. The CAM and CAF models have been used extensively to compute astronaut body organ exposures for the Space Shuttle and International Space Station programs.

ENVIRONMENTAL MODELS

The environments of concern are the LEO environment of ISS and the deep space (beyond the geomagnetic field) environment. They differ on account of the geomagnetic field. Although the Galactic Cosmic Rays are part of the over all exposure, only the trapped radiations during quiet geomagnetic periods will be considered in LEO and the solar particle events in deep space.

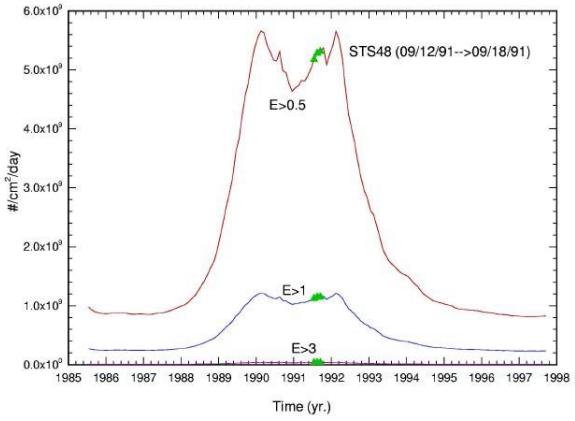

Fig. 5. STS-48 electron environment.

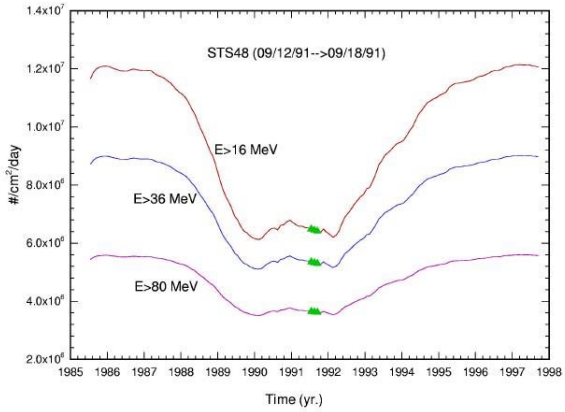

Fig.6. STS-48 proton environment.

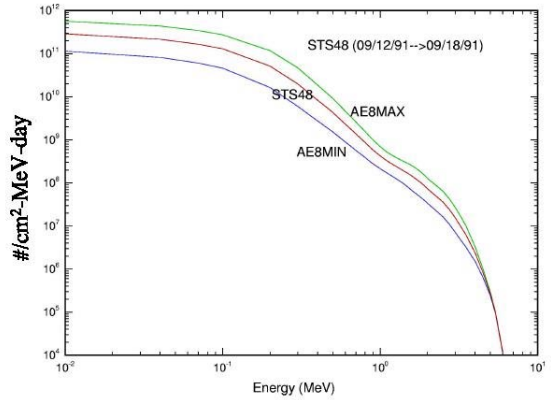

Fig.7. STS-48 electron environment compared to AE8 model.

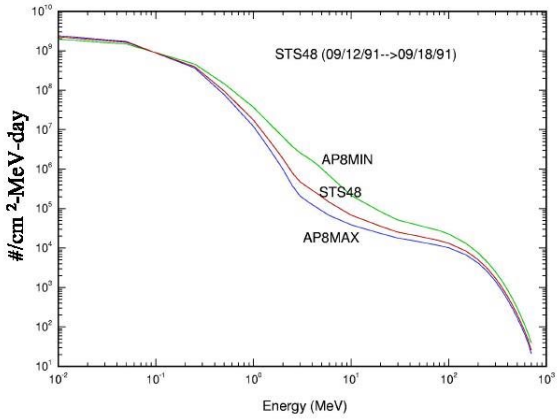

Fig. 8. STS-48 proton environment compared to AP8 model.

Even during geomagnetic quiet times the particle fields are variable over the solar cycle. The time dependent fields are shown relative to the Sept. 1991 flight environment of STS-48 at 313 nmi and 57^{o} in figures 5 and 6 as evaluated by a recently derived model [17]. The model utilizes the environmental maps of AE8 and AP8 with superimposed solar cycle variations related to particle source and loss terms. The STS-48 spectra during Sept. 1991 are compared to the base models at solar maximum and minimum in figures 7 and 8. The galactic cosmic ray background will be ignored in the present calculation. The solar energetic particles are deflected in the geomagnetic field and will be ignored in the present study although they can be an important contribution especially during geomagnetic storms [1]. Even more common and troubling are large geomagnetic disturbances and the associated increase in the trapped electron environment by three or four orders of magnitude lasting for several days.

Solar particle events in deep space operations are of great concern since a lethal exposure can be received over a several hour period [18] and the resultant biological response will be serious. This is especially true in a spacesuit where only minimal protection is available [18]. The largest observed high-energy event is that of Feb. 23, 1956 with the second largest such event being an order of magnitude smaller occurring on Sept. 29, 1989. The Feb. 23, 1956 event was only observed on the ground and the spectrum at low energies is most uncertain. It has been suggested that the Sept. 29, 1989 event where detailed measurements exists should be scaled by perhaps a factor of 10 and used as the event appropriate for design. Studies have shown that such an event would provide a considerable health risk to the astronaut although an overly simplified spacesuit model was used [19]. The fluence spectra of the Sept. 29, 1989 event [19] are shown in figures 9 and 10.

The low-level galactic cosmic ray exposures appear as background and will be ignored in the present study. The present emphasis is on the short-term exposures although the background from the trapped particles in LEO during geomagnitic quiet times is evaluated to estimate the dose during large electron population variations under disturbed geomagnetic conditions.

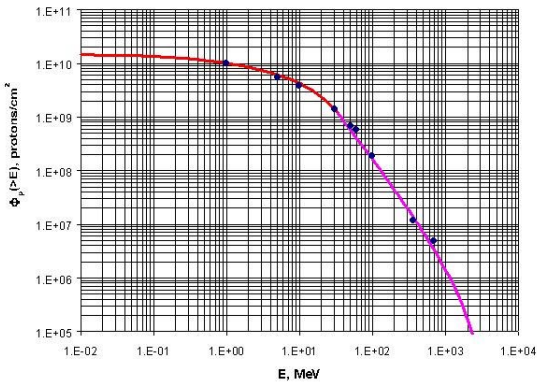

Fig. 9. Sept. 29, 1989 solar proton spectrum.

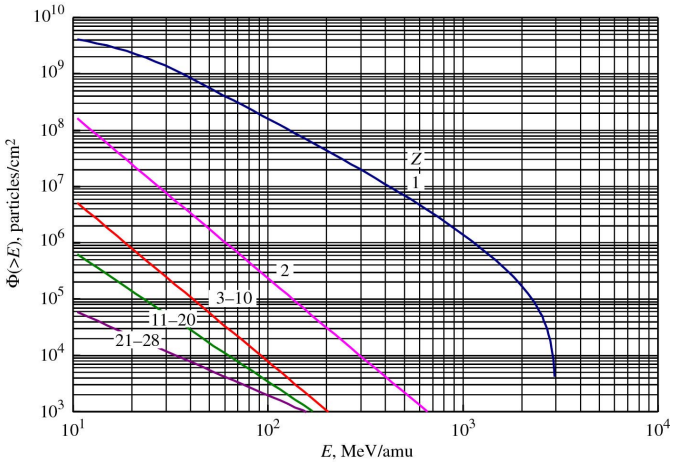

Fig. 10. Sept. 29, 1989 solar heavy ion spectra.

COMPUTATIONAL PROCEDURES

The types and energy distributions of particles transmitted through a shield material require the solution to the Boltzmann transport equation with appropriate boundary conditions related to the external space radiation environment. The relevant transport equation [20] for the flux density $\phi_j(\boldsymbol{x},\boldsymbol{\Omega},E)$ of type j particles moving in direction $\boldsymbol{\Omega}$ with energy E is given as

$$\boldsymbol{\Omega}\bullet\nabla\phi_j(\boldsymbol{x},\boldsymbol{\Omega},E) = \sum\int \sigma_{jk}(\boldsymbol{\Omega},\boldsymbol{\Omega}',E,E')\,\phi_k(\boldsymbol{x},\boldsymbol{\Omega}',E')\,d\boldsymbol{\Omega}'\,dE' - \sigma_j(E)\,\phi_j(\boldsymbol{x},\boldsymbol{\Omega},E) \quad (14)$$

where $\sigma_j(E)$ is the media macroscopic cross section for removal of j particles of energy E, $\sigma_{jk}(\boldsymbol{\Omega},\boldsymbol{\Omega}',E,E')$ are the media macroscopic cross sections for various atomic and nuclear processes adding j particles of energy E in direction $\boldsymbol{\Omega}$ including spontaneous disintegration. In general, there are hundreds of particle fields $\phi_j(\boldsymbol{x},\boldsymbol{\Omega},E)$ with several thousand cross-coupling terms $\sigma_{jk}(\boldsymbol{\Omega},\boldsymbol{\Omega}',E,E')$ through the integral in equation (14). The total cross section $\sigma_j(E)$ with the medium for each particle type of energy E may be expanded as

$$\sigma_j(E) = \sigma_{j,at}(E) + \sigma_{j,el}(E) + \sigma_{j,r}(E) \quad (15)$$

where the first term refers to collision with atomic electrons, the second term is for elastic nuclear scattering, and the third term describes nuclear reactive processes and are ordered as $1{:}10^{-5}{:}10^{-8}$. This ordering allows flexibility in expanding solutions to the Boltzmann equation as a sequence of physical perturbative approximations. The atomic interactions are treated using energy moments in which the leading term is the usual continuous slowing down approximation. Special problems arise in the perturbation approach for neutrons for which the nuclear elastic process appears as the first-order perturbation and has been the recent focus of research [21].

The electrons have negligible nuclear reaction cross sections and are dominated by atomic and elastic processes. The basic electron transport is treated by invoking the Continuous-Slowing-Down-Approximation (CSDA), where the usual CSDA range has been modified parametrically to account for shortened path length due to multiple scattering. The practical ranges and corresponding range-energy relations are derived from the parameterizations of Tabata, et al. [22]. For an electron of initial energy E, its residual energy, W, after going distance t in an attenuating medium may be found by solving the equation

$$R(W) = R(E) - t \quad (16)$$

for W when the practical range $R(W) > 0$. Effects of energy fluctuations are incorporated using the energy dissipation formulation of Kobetich and Katz [23,24], in which actual energy dissipation, G, is expressed in terms of a transmission function, η, as

$$G = d(\eta W)/dt \quad (17)$$

The parameterizations for R and η have been based on numerous electron beam experiments for energy ranges and material elements applicable to space radiation calculations.

The dose at distance t for electron differential flux ϕ_e may then be expressed in terms of the initial and final energy spectra [25]

$$D(t) = \int G(E,t)\,\phi_e(E)dE = \int S(W)\,\phi_e(W)dW \quad (18)$$

where S is stopping power. In conformance with the CSDA, the emerging electron spectrum may then be expressed in terms of the initial spectrum as [25]

$$\phi_e(W) = \phi_e(E)G(E)S(E)/[S(W)]^2 \quad (19)$$

In passing through condensed matter, the decelerating electrons give rise to energetic photons (bremsstrahlung), which also contribute to the total energy deposition. The photon production may be expressed in terms of a differential cross-section, $\sigma(W,E')$, which represents a probability that an electron of energy W produces a photon of energy E' in its interaction with an atom of the material. These cross-sections are generally complicated functions of W, E', and material composition. They have been extensively tabulated by Seltzer and Berger [26] for wide energy ranges and most elements of the periodic chart. The effective production cross-sections for a given material are determined in the present calculations by appropriate spline interpolations of the Berger-Seltzer tabulations.

The photon source term, ς, at distance x and energy E' may be calculated from the electron spectrum as

$$\varsigma(x, E') = \int_{E'}^{W(x)} \phi_e\,\sigma(W, E')\,dW \quad (20)$$

The photons are also being attenuated in accordance with an extinction coefficient, μ, and the photon differential spectrum, $\phi_p(E')$, at distance t may be found using the transfer equation

$$\phi_p(E') = \int \varsigma(x, E')\, e^{-\mu(t-x)}\, dx \qquad (21)$$

and the subsequent energy deposition as

$$D_p(t) = \int \mu_e E' \phi_p(E') d E' \qquad (22)$$

where μ_e is an absorption coefficient for photon energy loss resulting in ionizing energy deposition (generally less than the total extinction coefficient, μ). The present code formulation assumes all photons generated propagate in the direction of electron motion.

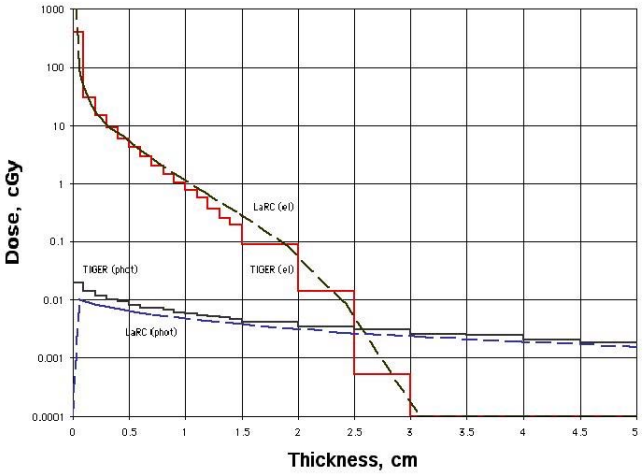

Fig. 11. STS-63 electron generated dose in a water shield of the present model and TIGERP.

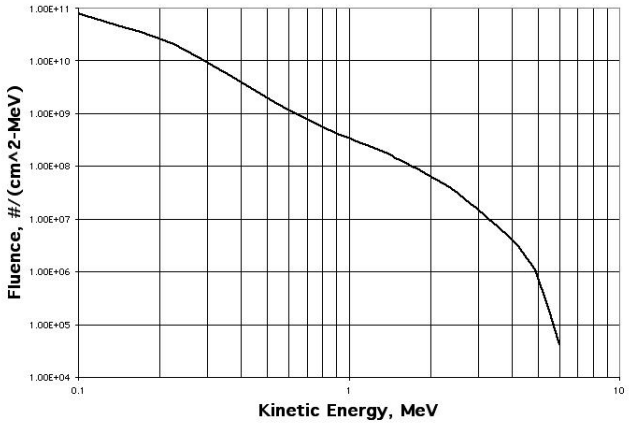

Fig. 12. Ten day electron fluence for STS-63.

This simple procedure is of recent vintage, and validation and benchmarking continue at the present time. Calculations for benchmark comparisons made thus far indicate that accuracy has not been substantially degraded at the expense of computational speed. An example of a comparison calculation is given in figure 11 for the electron fluence spectrum shown in figure 12 appropriate to the STS-63 10-day mission at 213 nmi (392 km) at 51.6° inclination and is propagated at normal incidence through a semi-infinite water slab. The Monte Carlo code TIGERP [27] was used to validate the computation and the very favorable comparison is evident.

RESULTS

The dose at a location within the astronaut's body depends on the surrounding spacesuit materials and body tissues. The spacesuit material distributions are evaluated along 1922 ray directions associated with a fixed solid angle ($\Delta\Omega = 4\pi/1922$) as discussed elsewhere [28]. Various 3D visualization techniques are useful in understanding these distributions. For example, the projected rays through the spacesuit materials about a location in the sternum are shown in figure 13. The potential role of the EMU Lights and camera, the backpack, and the Display Control Module (DCM) are clearly evident.

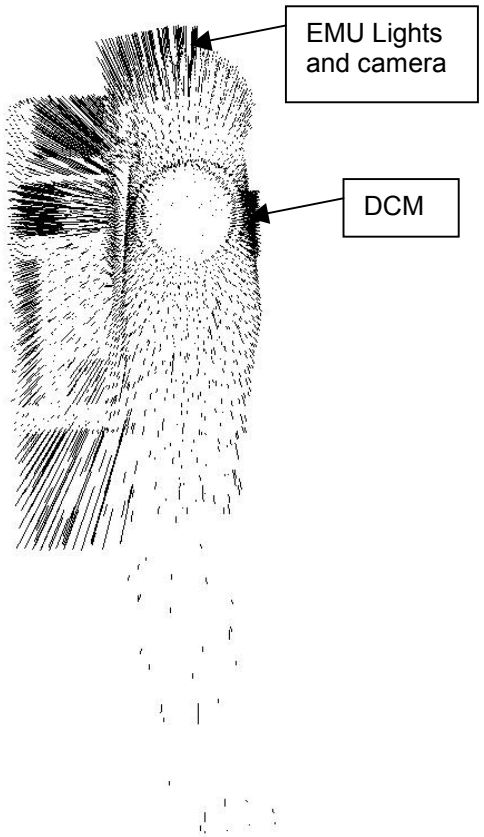

Fig. 13. Projected spacesuit material crossings along 1922 ray directions.

Another visualization technique is shown in figure 14 where the gray scale (normally color is used) displays the relative shielding about the dose point. For online analysis, the spherical shape in figure 14 is rotated to fully examine the total solid angle. The power of such analysis techniques is further discussed by Qualls and Boykins [28] and provides a basic tool for design analysis and optimization.

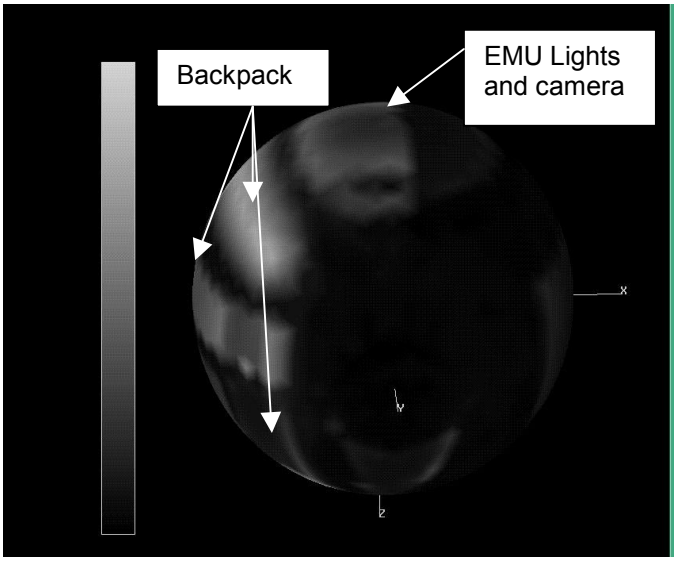

Fig. 14. Visualization of the spacesuit shield materials distribution about a point in the sternum.

The environments of concern are the LEO environment of ISS and the deep space environment. They differ on account of the geomagnetic field. Although the Galactic Cosmic Rays are part of the over all exposure, only the trapped radiations during quiet geomagnetic periods will be considered for LEO and the modeled Sept. 1989 solare particle event will be used for operations on the lunar surface.

LEO OPERATIONS – The trapped environment near solar maximum is shown in figures 5 through 8 for this high inclination and relatively high altitude orbit. The attenuation of that environment is shown in figures 15 to 18 for low penetration depths. Figures 16 and 17 exhibit sample differential electron and photon energy spectra for the electron transport code applied to the modeled EMU fabric for the nominal thickness and twice that thickness. The electrons are stronly attenuated over relatively small distances, whereas the photons are shown to have a slight increase over much of the energy range, indicative of their more penetrating nature. One can see from figures 15 and 18 that the doses can be quite high for low penetration depths and reduce quickly with increasing depth. The basal layer of the skin lies about 1 mm below the surface and the additional 0.28 g/cm^2 of fabric used in prior calculations would result in about 6 cGy per day from electrons, neglecting selfshielding. The present estimate of the mean fabric penetration is 0.161 g/cm^2 with resultant exposures on the order of 14 cGy/day or more than a factor of two higher than results for the prior model. The relative difference between the two fabric models will remain although selfshielding will lower the total dose considerably. Although the protons likewise attenuate quickly at low penetration depths, the resultant exposure is not as large as that for electrons.

The dose incurred during a six-hour exposure for geomagnetic quiet times near solar maximum is not to be expected to be a serious limiting factor. However, geomagnetic storms are observed during solar active years to increase the electron environment, over a period of approximately an hour or less, by three or four orders of magnitude greater than the quiet time levels shown in figures 5 and 15. Even a modest amount of time in such an environment can lead to serious exposures, especially to the skin. The thresholds for the early radiation responses (deterministic effects as opposed to the stochastic effects such as cancer induction) are very narrow functions of exposure and a factor of two difference in exposure is extremely important to radiation health outcome [18,29].

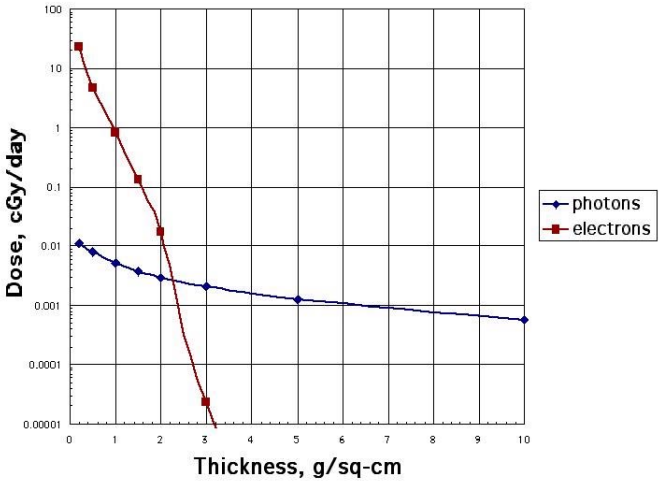

Fig. 15. STS-48 electron and photon dose as a function of fabric thickness.

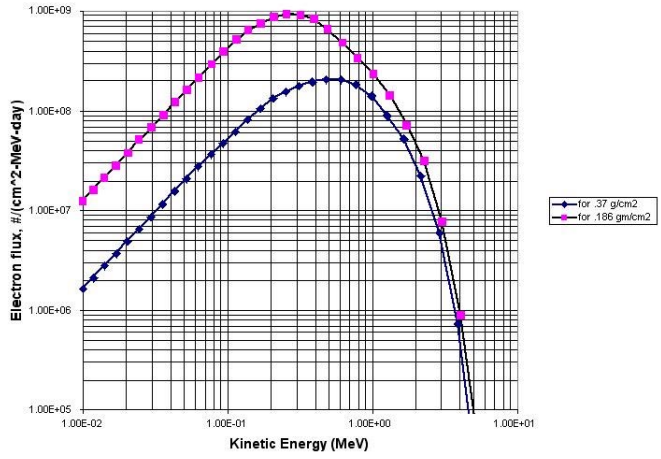

Fig. 16. Sample spectra for LEO electrons in spacesuit fabric.

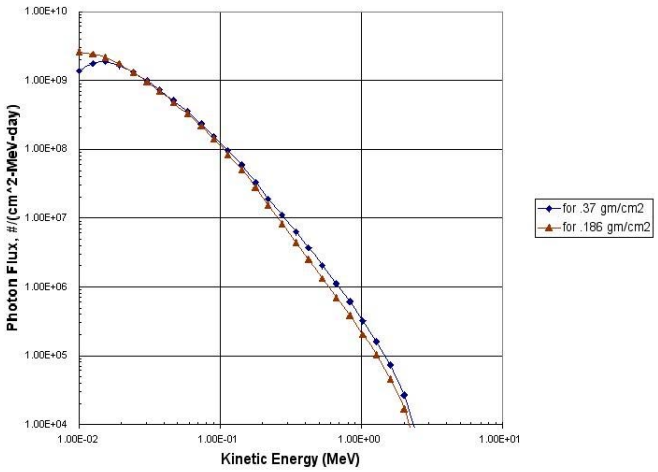

Fig. 17. Photon spectra generated by electrons in spacesuit fabric.

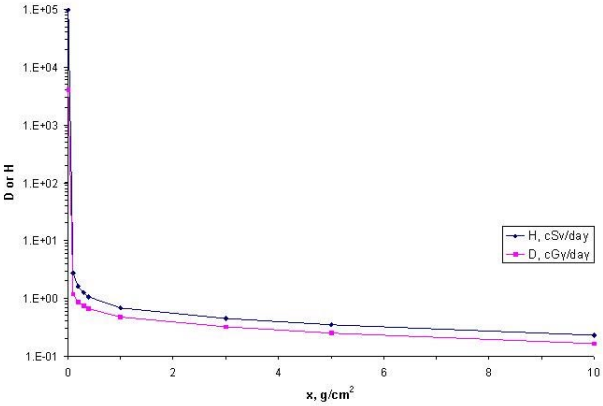

Fig. 18. STS-48 proton daily dose and dose equivalent as a function of fabric thickness.

Two CAM body points have been chosen to demonstrate typical computational results: a skin exposure point in the lower right shin and a point on the right ocular lens. The spacesuit material in close proximity to the leg point is taken as a single layer of mean areal density of 0.185 g/cm^2 (composition 48% C, 42% H, 9% O by mass). For the lens point the helmet was modeled by a single polysulfone layer (50% C, 40.7% H, 7.4% O, 1.9% S). For the sample calculations shown here, EMU thicknesses encountered along rays emanating from the dose target point were scaled to equivalent thickness of these two materials. The associated body tissue thicknesses were scaled according to the same materials.

Figure 19 is given to illustrate some of the directional characteristics of the exposures obtained from the combined EMU CAD model enclosing the CAM body model. The CAM coordinates are fundamentally a Cartesian right-hand system with origin at top of head and vertical distances increasing downward. The positive directions of the x and y axes are forward and through the right shoulder, respectively. In the usual spherical coordinate representation (polar angle θ, azimuth φ), the CAM model formulation used in the present analysis consists of 968 directions (22 polar angles θ and 44 evenly distributed azimuth angles associated with each θ). The increasing thickness of penetration for directions away from the normal of the spacesuit fabric is clearly seen.

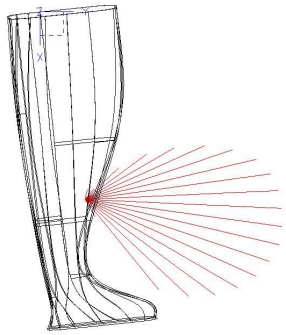

Fig. 19. Directional dose variation for the right shin target point.

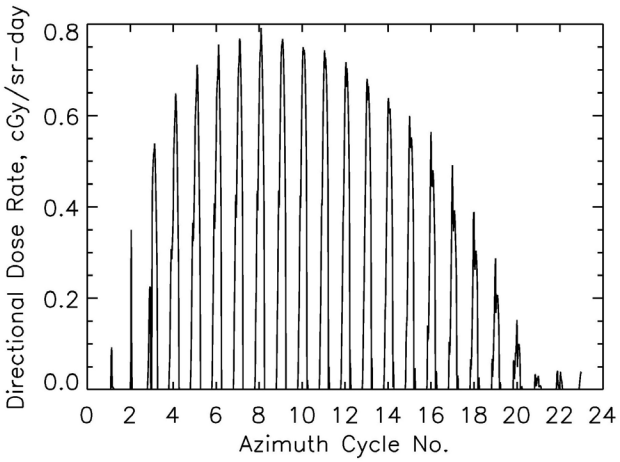

Fig. 20 Directional dose values for the right shin target point.

The ray patterns are depicted for the sequence of polar angles in an x-z plane, with length of rays proportional to directional dose magnitudes. The leg point is indicative of exposure from the LEO trapped electrons from the orbit-averaged STS-48 mission. The entirety of directional dose values about the selected CAM target points are plotted in figure 20. Similar results are given in figure 21 for the right ocular lens within the helmet. The abscissas of the plots may be considered as quasi-2D, with each polar angle represented by the values calculated for its associated azimuth sweep - hence the cyclic nature of the plotted values. The peak values for each cycle are indicative of the direction in which the target point is nearest the surrounding spacesuit material. (Note that the increasing azimuth cycle number in the plots show progression of the polar angle from downward to upward direction, i. e., CAM toe -> CAM head). In figure 21, the sudden drop in cyclic peak values above the horizontal (about cycle 11) is a result of

the added attenuation of the LEO electrons by the helmet visor.

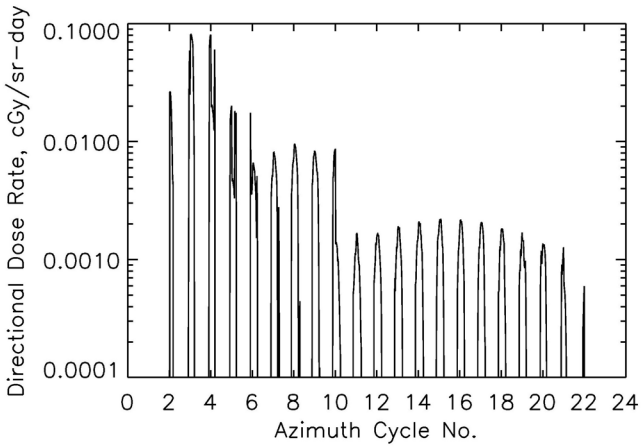

Fig. 21. Directional dose values for the right ocular lens target point.

It is recognized that the information displayed in figures 15 - 21 do not represent end-point results of a complete dosimetric calculation, but it is felt that such diagnostic checks are essential in validating the complex procedures involved in making complete analyses that usually require a vast number of essentially repetitive operations. For the two target points discussed herein, the resultant integrated dose values are given in table 5.

In the event of a large geomagnetic storm, the electron fluence is seen to increase upto four orders of magnitude in less than an hour. In this case, the lens and skin dose rate would increase by such a factor (and may be more penetrating due to acceleration processes). These high rates are likewise given in table 5. It is clear that potentially large exposures can occur during such periods and timely shelter in the ISS is required during such periods.

DEEP SPACE OPERATIONS – There are two issues in deep space exposures: the rates of cancer induction from galactic cosmic rays and concern for a solar particle event. Solar particle events are of potentially grave concern in space exploration where astronauts will spend periods in poorly protected regions as the spacesuit. The August 4, 1972 solar particle event is the worst case event (for space exposures) for which some details of the low energy proton spectrum were measured and used to analyze their importance to astronaut health [18]. The single largest ground level event observed is the February 23, 1956 event but little is known of the low energy spectrum. The second largest ground level event observed is the September 29, 1989 and good details on the spectral properties [19] are available as shown in figures 9 and 10. The importance of the September 29, 1989 event which we evaluate herein is that ten times the September 29, 1989 event is a proxy for the February 23, 1956 event (the largest ground level event so far observed).

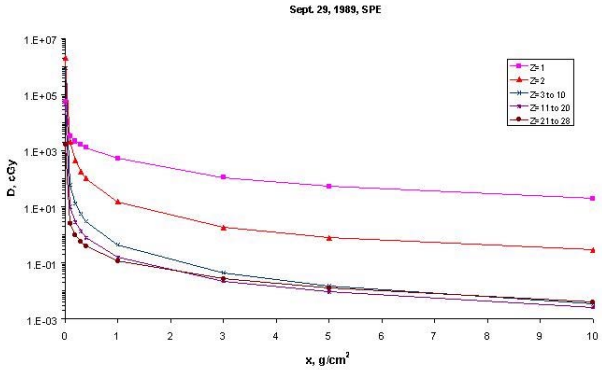

Fig. 22. Dose within a fabric shield during the September 29, 1989 SPE.

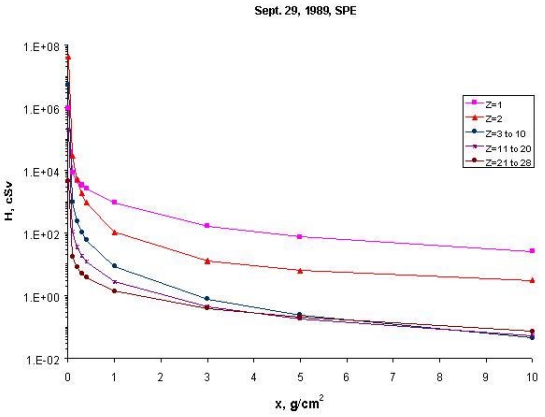

Fig. 23. Dose equivalent within a fabric shield during the September 29, 1989 SPE.

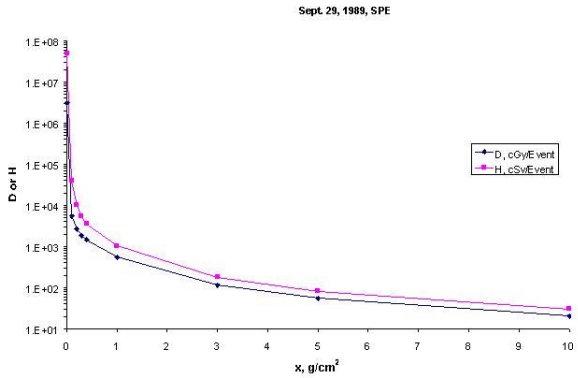

Fig. 24. Total dose and dose equivalent within a fabric shield during the September 29, 1989 SPE.

The dose and dose equivalent in tissue from various components within a spherical shell of spacesuit fabric material is shown in figures 22 and 23 with the totals in figure 24. The dose is dominated by the proton fluence over most shielding thickness. The dose equivalent from

helium ions gives an important contribution for thickness on the order of the spacesuit fabric. The heavier ions are always unimportant to the exposure.

It is clear from the results in figure 24 that very high skin exposures can be expected for this event. However, even modest amounts of additional shielding in the Thermal Micrometeoroid Garment (TMG) and LCVG are expected to have important effects in reducing the exposures. Still some caution in redesign is warranted since mobility and comfort to the astronaut is a key issue in space operations. There is a slow but significant decline in dose and dose equivalent with larger shield thickness indicating some advantage is to be gained by the more massive components of the suit and the self shielding of critical tissues of the astronauts body. These will be evaluated in terms of the CAM/CAF geometry and the present spacesuit model.

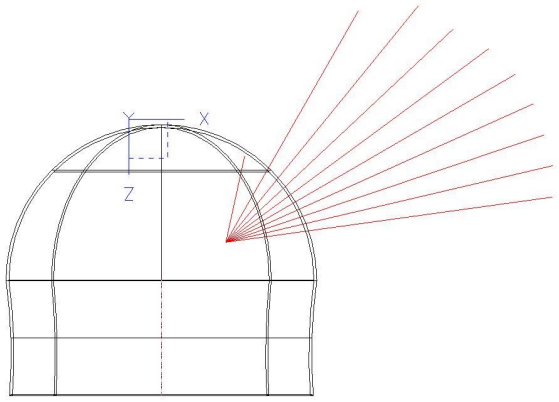

Fig. 25. Directional dose variation for the right ocular lens through helmet material for the Sept. 1989 SPE.

Table. 5. Integrated dose values for the lens and leg-skin target points.

Source/Target	Lens Dose	Leg-skin Dose
Trapped e^-, cGy/d	0.026	1.69
Photons, cGy/d	0.0014	0.0032
Storm e^-, cGy/d	260.	1,690
Storm photons, cGy/d	1.4	3.2
Sept. 1989 SPE (lunar surface), cGy/d	82.7	412.

Figure 25 is given to illustrate some of the directional characteristics of the exposures obtained from the combined EMU CAD model enclosing the CAM body model on the lunar surfaceduring the Sept. 1989 SPE for the right ocular lens. The right ocular lens dose is derived from the SPE spectrum for a lunar surface exposure, with the evident planetary shielding resulting in essentially no dose contribution below the horizontal. The ray patterns are depicted for the sequence of polar angles in an x-z plane, with length of rays proportional to directional dose magnitudes. The degree of attenuation with increasing azimuth is slight due to the curvature of the helmet relative to the lens location. The total exposures for the Sept. 1989 SPE at the right ocular lens and skin of the shin is given in table 5.

CONCLUSION

All of the computational elements described here are available for detailed and comprehensive astronaut space radiation exposure evaluations for EVA scenarios. Code validation and streamlining have been performed to the extent that full implementation with the space suit/CAM combination may be carried out for a distribution, or grid, of target points throughout the configuration. As of now, no special effort has been made to assess run-time for such an application, but a rough estimate for generating a reasonably complete body exposure dose map (~150 CAM target points) may be carried out in a matter of minutes in serial calculation on a machine with moderate computational speed. Execution on parallel-processing machines should greatly reduce run times, and plans are in place to provide a source code version that takes advantage of parallel-processor implementation.

The purpose for the present development of the EMU-CAM configuration coupled with the radiation transport codes is to provide a means for generating accurate and comprehensive exposure evaluations in a time-frame that allows a more-or-less immediate, as opposed to after-the-fact, application. For example, scenarios with time-varying external environments may be examined quickly; impact of EMU modifications on shielding properties may be assessed and/or optimized. In a specific analysis, the time consumed in I/O set-up will usually be far greater than procedure execution itself, and routine validation diagnostics (usually consisting of optional ancillary calculations), are of paramount importance. Such diagnostic procedures have been incorporated in the formulation in order that they may be readily activated when configuration or I/O structures are modified.

It is clear from the present analysis and results that the spacesuit has some important features which will have some benefit for reducing the astronaut health risks under the extreme exposure conditions in space. Even so there is some weakness in the spacesuit design which is already clear. Mainly the attention has been presently been given to the spacesuit fabric (TMG/LCVG) which is less effective in protecting the skin from exposure than previously assumed and could be greatly improved. It is clear that only modest additions to the fabric elements will have a large payoff in protection. What still needs addressed is the remainder of more massive elements within the spacesuit and their effects

on specific critical organ tissue exposures. This will be more fully addressed in the near future.

REFERENCES

1. Nealy, J.E. et al. Adv. Space Res. 17(2): 117-120, 1996.
2. Kozloski L.D., US Space Gear: Outfitting the Astronaut, Smithsonian Institution Press, Washington DC, 1994.
3. Severin G.I., Acta Astronautica 32(1): 15-23, 1994.
4. Abramov I.P., Acta Astronautica 36(1): 1-12, 1995.
5. Kosmo J.J., Nachtwey D.S., Hardy A. JSC/CTSD-SS-241, 1-24-1989.
6. Ross A.J. et al. NASA CP 3360, 1997.
7. Wilson, J.W. SAE 01ICES-2372, 2001.
8. Wilson, J.W. Health Phys. 28:812-813, 1975.
9. Wilson, J.W. et al. NASA TP-3668, 1997.
10. Kase, Paul G., "Computerized Anatomical Model Man, " Report AFWL-TR-69-161, Air Force Weapons Laboratory, Kirtland Air Force Base, NM, January 1970.
11. Billings, M.P., and W.R. Yucker, "Summary Final Report. The Computerized Anatomical Man (CAM) Model," Report MDC G4655, McDonnell Douglas Astronautics Company, Huntington Beach, CA, September 1973.
12. Jordan, T.M., "QUAD, A Computer Subroutine for Ray Tracing in Quadric Surface Geometries," Douglas Report SM-46333, 1964.
13. Yucker, W.R., and S.L. Huston, "Computerized Anatomical Female. Final Report," Report MDC H 6107, McDonnell Douglas Corporation, Huntington Beach, CA, September 1990.
14. Yucker, W.R., "Computerized Anatomical Female Body Self-Shielding Distributions," Report MDC 92H0749, McDonnell Douglas Corporation, Huntington Beach, CA, March 1992.
15. Atwell, W., "Anatomical Models for Space Radiation Applications: An Overview;" Invited paper (F2.4-M.1.06) presented at the Committee on Space Research (COSPAR), Washington, DC, August 28 - September 5, 1992.
16. Atwell, W., A. C. Hardy, and L. Peterson, "Organ Radiation Doses and Lifetime Risk of Excess Cancer for Several Space Shuttle Missions," Invited paper # F2.4-001, Committee on Space Research (COSPAR), Hamburg, Germany, July 11-21, 1994.
17. Wilson, J.W. et al. NASA/TP-1999-209369, 1999.
18. Wilson, J.W. et al. Radiat. Measurment 30: 361-382; 1999.
19. Kim, H.-Y. M. et al. NASA TP/1999-209320, 1999.
20. Wilson, J. W. et al., *Transport Methods and Interactions for Space Radiations.* NASA Reference Publication, RP-1257, 1991.
21. Clowdsley, M. S. et al., Cana. J. Phys. 78: 45-56, 2000.
22. Tabata, T., et al., Nucl. Inst. & Meth. 103: 85-91, 1972.
23. Kobetich, E. J. and Katz, R., Nucl. Inst. & Meth. 71: 226-230, 1969.
24. Kobetich, E. J. and Katz, R., Phys. Rev. 170(2): 391-396, 1968.
25. Cucinotta, F.A.; Katz, R.; and Wilson, J.W.: Radial Distributions of Electron Spectra From High-Energy Ions. Radiat. Environ. Biophysics 37:259-265; 1998
26. Seltzer, S. M. and Berger, M. J., Nucl. Inst. & Meth. B12: 95- , 1985.
27. Halbleib, J. A. and Morel, J. E., Nucl. Sci. Eng., 70: 219- , 1979
28. Qualls, G.D. and Boykins, R., Space Radiation Shielding Analysis by CAD Techniques. NASA CP 3360, pp. 365-382; 1997.
29. NCRP, Guidance on Radiation Received in Space Activity, NCRP Report No. 98, 1989.

CONTACT

B.M.ANDERSON@LARC.NASA.GOV